Metrology with entangled states

M. W. Mitchell

Institut de Ciències Fotòniques, C/ Jordi Girona, 29. Building Nexus II , 08034 Barcelona, Spain

ABSTRACT

It is well known that classical states of light exhibit shot noise, characteristic of independent or uncorrelated particles. For phase estimation problems, this leads to a shot-noise limited uncertainty of 1/sqrt[N], where N is the number of particles detected. It is also well known that the shot-noise limit is not fundamental: squeezed states and entangled states can be used for sub-shot-noise phase measurements. The fundamental or "Heisenberg" limit is set by the uncertainty principle: the minimum possible uncertainty in phase is 1/N.

We have recently demonstrated a method, using parametric downconversion and post-selection, to generate entangled "NOON" states suitable for sub-shot-noise phase measurements [M.W. Mitchell et al, Nature 429, 161 (2004)]. We generated a three-photon NOON state and demonstrated three-fold improvement in phase resolution with this state.

The relationship between phase resolution and phase uncertainty depends on prior information about the phase being estimated. As in the case of phase measurements with squeezed states, extra precision in one dimension is gained at the cost of reduced precision in other dimensions. Only when prior information is incorporated can entangled-state metrology be applied to beat the shot-noise limit. We illustrate this relationship and discuss adaptive strategies for phase estimation and the possibility of reaching the Heisenberg limit.

Keywords: Entanglement, state preparation, metrology, phase estimation

1. INTRODUCTION

Interference and interferometers have been employed to perform precise measurements at least since Fraunhofer developed the diffraction grating and observed spectral lines in sunlight. Today the most precise and demanding measurements are often performed as interference measurements. A few examples include Ramsey interferometry in atomic spectroscopy,[1] x-ray diffraction in crystallography[2] and optical interferometry in gravitational-wave studies.[3,4] These experiments can be understood as measurement of an externally-imposed and essentially classical phase, for example the phase from a passing gravitational wave, by observing its effect upon a quantum system or a collection of quantum systems. Quantum mechanics thus sets fundamental limits on the precision with which the classical phase can be determined. For independent quantum systems, shot noise limits the phase uncertainty to $\delta\phi \geq 1/\sqrt{N}$ where N is the number of (2-state) systems used, but it is known that entangled systems can beat this limit. The uncertainty principle sets a fundamental precision limit of $\delta\phi \geq 1/N$, known as the "Heisenberg limit."

In this paper we consider phase measurements using a type of maximally entangled N-photon state called a "NooN" state. This state shows a phase resolution N times better than a single-photon state. We demonstrate a technique for producing polarization NooN states, applicable to arbitrary N, and show the expected increase in phase resolution. We also consider the utility of such states for estimation of unknown phases. We show that sequential, adaptive use of NooN states in phase estimation can achieve the Heisenberg-limit scaling of $\delta\phi \propto 1/N$.

Further author information: (Send correspondence to M.W.M.)
M.W.M.: E-mail: morgan.mitchell-at-icfo.es

2. "NOON" STATE GENERATION

It has been known for some time that entangled states can be used to perform super-sensitive measurements, for example in optical interferometry or atomic spectroscopy.[5–9] The idea has been demonstrated for an entangled state of two photons,[10] but for larger numbers of particles it is difficult to create the necessary multi-particle entangled states.[11–13] Here we experimentally demonstrate a technique for producing a maximally-entangled three-photon state from initially non-entangled photons. The method can in principle be applied to generate states of arbitrary photon number, giving arbitrarily large improvement in measurement resolution.[14–17] The method of state construction requires non-unitary operations, which we perform using post-selected linear-optics techniques similar to those used for linear-optics quantum computing.[18–22]

Our goal is to create the state

$$|N::0\rangle_{a,b} \equiv \frac{1}{\sqrt{2}}\left(|N,0\rangle_{a,b} + |0,N\rangle_{a,b}\right) \tag{1}$$

which describes two modes a, b in a superposition of distinct Fock states $|n_a = N, n_b = 0\rangle$ and $|n_a = 0, n_b = N\rangle$. This state figures in several metrology proposals, including atomic frequency measurements,[6] interferometry,[5,7,9] and matter-wave gyroscopes.[8] In these proposals the particles occupying the modes are atoms or photons.

The advantage for spectroscopy can be seen in this idealization: We wish to measure a level splitting $H_{ext} = \varepsilon_{ba} b^\dagger b$ between modes b and a using a fixed number of particles N in a fixed time T. We could prepare N copies of the single-particle state $(|1,0\rangle_{a,b} + |0,1\rangle_{a,b})/\sqrt{2}$ and allow them to evolve to the state $|\phi\rangle \equiv (|1,0\rangle_{a,b} + \exp[i\phi]\,|0,1\rangle_{a,b})/\sqrt{2}$, where $\phi = \varepsilon_{ba}T/\hbar$. Measurements of $A_1 \equiv |0,1\rangle\langle 1,0| + |1,0\rangle\langle 0,1|$ on this ensemble give $\langle A_1\rangle = \cos(\phi)$ with phase uncertainty at the shot-noise limit, $\Delta\phi = 1/\sqrt{N}$. In contrast, under the same Hamiltonian $|N::0\rangle$ evolves to $(|N,0\rangle + \exp[iN\phi]\,|0,N\rangle)/\sqrt{2}$. If we measure the operator $A_N \equiv |0,N\rangle\langle N,0| + |N,0\rangle\langle 0,N|$, we find $\langle A_N\rangle = \cos(N\phi)$. The dependence on $N\phi$ rather than ϕ is phase *super-resolution*: one cycle of $\langle A_N\rangle$ implies a smaller change of ϕ (or ε_{ba}) than one cycle of $\langle A_1\rangle$. Phase *super-sensitivity*, a reduction of phase uncertainty, is also predicted. A number of schemes have been proposed[5–9,14,23,24] to reach the so-called Heisenberg limit $\Delta\phi = 1/N$. The simplest proposals would measure the operator A_N. This can be implemented with coincidence measurements, as the probability of detecting all N quanta in a mode $(a+b)/\sqrt{2}$ is proportional to $1 + \langle A_N\rangle$. Phase super-resolution has been demonstrated for $N = 2$ with photons in a Mach-Zehnder interferometer[25,26] and with trapped ions.[27]

A related technique, quantum interferometric optical lithography, proposes using phase super-resolution to write features smaller than the single-photon diffraction limit. There the modes a, b are spatial, with different propagation directions. A molecule exposed to both modes and capable of absorbing N photons would, in effect, perform the measurement of A_N as above, with N-fold super-resolution in position. Using coincidence detection in place of two-photon absorbers, this principle has been demonstrated for $N = 2$ using down-converted pairs.[10] In that experiment, as well as in the earlier Mach-Zehnder experiments, two infrared photons showed the same resolution or angular resolution as the blue pump photon which generated them, a factor of two improvement over the resolution of a single infrared photon. The question remains as to whether resolution can be improved beyond that of the photons used to generate the entangled state. Here we answer that question in the affirmative by constructing a multi-particle state with greater phase resolution than any of its single-particle precursors. The technique could in principle be used to generate entangled states of arbitrarily large N with arbitrarily good resolution.

We prepare the state $|3::0\rangle_{a,b}$ where the modes a and b are the horizontal (H) and vertical (V) polarizations of a single spatial mode. The construction of the polarization state is based on earlier proposals to construct photon-number path entangled states.[14–16] A similar technique for polarization has recently been independently proposed.[17] The key to the construction is the fact that $|3::0\rangle_{a,b}$, when written in terms of creation operators $a_a^\dagger$ and $a_b^\dagger$ acting on the vacuum $|0\rangle$, is

$$|3::0\rangle_{a,b} = (a_a^\dagger + a_b^\dagger)(a_a^\dagger + e^{i\chi}a_b^\dagger)(a_a^\dagger + e^{i2\chi}a_b^\dagger)\,|0\rangle \tag{2}$$

where $\chi = 2\pi/3$ and normalization has been omitted. The terms in parentheses each create a particle, but in non-orthogonal states. If a and b are left and right circular polarization, these states describe linear polarizations

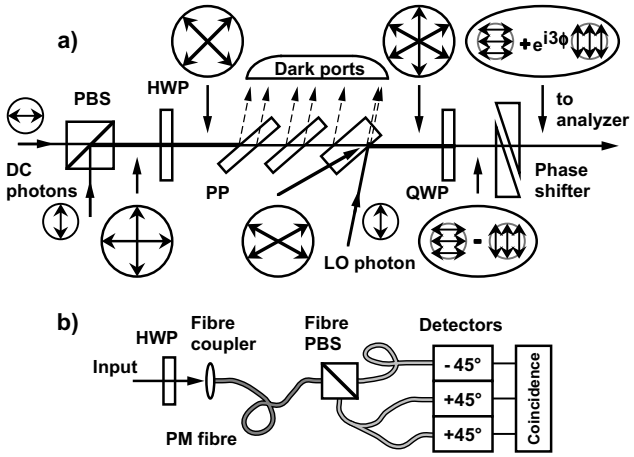

Figure 1. Schematic of production and detection of the state $|3::0\rangle^{3\phi}_{H,V}$. Part a) shows the chain of optical components and their effect on polarization state, represented in encircled figures. All photons have wavelength 810 nm. A polarizing beamsplitter (PBS) puts the DC photons in a single spatial mode and a half wave-plate (HWP) rotates their polarizations to $\pm 45^\circ$. A partial polarizer (PP) transforms the polarizations to $\pm 60^\circ$ if no photons are reflected into the dark ports. The LO photon is injected at the final interface of the partial polarizer. A quarter wave-plate (QWP) rotates to $(|3,0\rangle_{H,V} - |0,3\rangle_{H,V})/\sqrt{2}$ and quartz wedges produce an adjustable phase 3ϕ between the two components of the state. b) analysis in the $\pm 45^\circ$ polarization basis is performed with a HWP before a polarization-maintaining (PM) fibre and a fibre-coupled PBS. The outputs of the fibre PBS are channeled to one, two, or three detectors as needed. The configuration to detect $|2,1\rangle_{\pm 45^\circ}$ is shown. Digital electronics record single detections as well as two- and three-fold coincidences.

rotated by 60° from each other. Using post-selection, we can put one photon of each polarization into a single spatial mode and create $|3::0\rangle_{a,b}$.

We use two photons from pulsed parametric down-conversion plus one laser, or "local oscillator" (LO) photon, adapting a technique first used to show non-classical interference of independent sources.[28, 29] Pulses of 100 fs duration and 810 nm center wavelength are produced by a mode-locked Ti:sapphire laser and frequency-doubled giving 405 nm pulses with an average power of 50 mW. These are gently focused into a 0.5 mm thick beta-barium borate crystal aligned for Type-II parametric down-conversion in the "collapsed cone" geometry.[30] The down-converted (DC) photons thus produced are orthogonally polarized. A small part of the Ti:sapphire beam is split off and attenuated to contribute the LO photon. These three photons are transformed into the state $|3::0\rangle$ and detected by polarization-resolved three-fold coincidence detection. The transformation, shown in Figure 1 a), can be understood as a sequence of mode combinations. After the PBS, the DC photons are in the state $a^\dagger_H a^\dagger_V |0\rangle$, where subscripts indicate polarization. A half wave-plate rotates this to $a^\dagger_{+45^\circ} a^\dagger_{-45^\circ} |0\rangle$ where subscripts show linear polarizations measured from vertical. We perform the first post-selected non-unitary operation by passing the pair through three plates of BK7 glass near the Brewster angle. The six Brewster-angle interfaces act as a partial polarizer (PP) with transmission efficiencies of $T_H \approx 1$, $T_V = 1/3$. By post-selecting cases where no photons are reflected, we transform the state as (again without normalization)

$$\begin{aligned} a^\dagger_{+45^\circ} a^\dagger_{-45^\circ} |0\rangle &= (a^\dagger_H + a^\dagger_V)(a^\dagger_H - a^\dagger_V) |0\rangle \\ &\rightarrow (a^\dagger_H + \frac{1}{\sqrt{3}} a^\dagger_V)(a^\dagger_H - \frac{1}{\sqrt{3}} a^\dagger_V) |0\rangle \\ &= a^\dagger_{+60^\circ} a^\dagger_{-60^\circ} |0\rangle . \end{aligned} \tag{3}$$

This operation, putting orthogonally polarized photons into non-orthogonal modes, is non-unitary and requires post-selection.

The DC photons meet the LO photon at the last interface of the PP. This interface acts as a beamsplitter putting all three into the same spatial mode, conditioned on zero photons exiting by the "dark" port. Again,

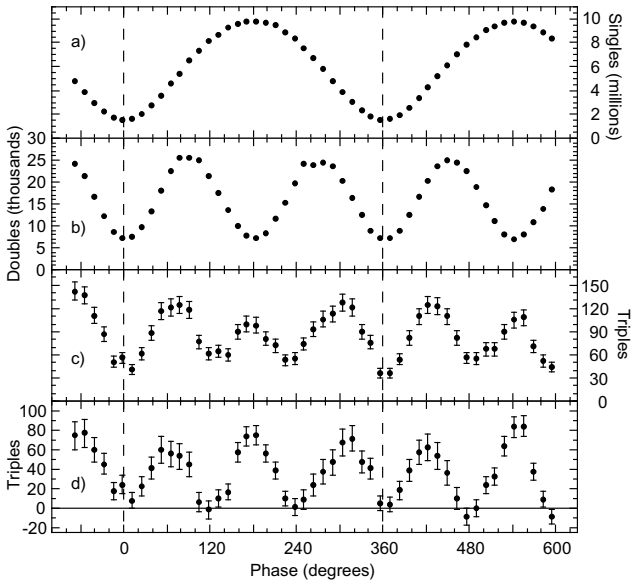

Figure 2. Super-resolving phase measurement with two and three photons. The polarization analyzer is configured with one detector on the -45° output and two on +45° . The input, a combination of down-converted and laser photons, is constructed to give the state $|3::0\rangle_{H,V}^{3\phi}$ upon post-selection (see text). All graphs show detections per 30 second counting interval as the phase ϕ is changed by translating a phase-shifter prism. a) singles detection at -45° , i.e., detection of $|0,1\rangle_{\pm 45^\circ}$, shows oscillation with ϕ. b) two-fold coincidence detection of $|1,1\rangle_{\pm 45^\circ}$ shows oscillation with 2ϕ. c) three-fold coincidence detection of $|2,1\rangle_{\pm 45^\circ}$ shows oscillation with 3ϕ. Error bars indicate $\pm\sigma$ statistical uncertainty. d) three-fold coincidence after background subtraction. Error bars show $\pm\sigma$ statistical uncertainty plus a systematic uncertainty in the background. Dashed vertical bars indicate one full cycle.

the operation is non-unitary and requires post-selection. The LO photon is vertically polarized and the state thus constructed is $a^\dagger_{0^\circ} a^\dagger_{+60^\circ} a^\dagger_{-60^\circ} |0\rangle$. This state has six-fold rotational symmetry about the beam propagation direction, and thus can only contain the states $|3,0\rangle_{L,R}$ and $|0,3\rangle_{L,R}$ where subscripts indicate the circular polarization basis.[17] In fact, it is easily verified that the state is $(|3,0\rangle_{L,R} - |0,3\rangle_{L,R})/\sqrt{2}$ up to an overall phase. Finally, we convert circular to linear polarizations with a quarter wave-plate, giving $(|3,0\rangle_{H,V} - |0,3\rangle_{H,V})/\sqrt{2}$. Ideally, the probability of both post-selections succeeding is $2\cos^4(\pi/12)/3 \approx 58\%$.

Response to the phase shifter demonstrates phase super-resolution. Acting on a single photon, the quartz wedges shift by ϕ the phase of the V-polarization. Acting on three photons the phase shift is tripled: $|3::0\rangle_{H,V}$ becomes $|3::0\rangle_{H,V}^{3\phi} \equiv (|3,0\rangle_{H,V} + \exp[i3\phi]\,|0,3\rangle_{H,V})/\sqrt{2}$, where we have absorbed the negative sign above into the phase factor. The 3ϕ behaviour can be seen in triples detection in the $\pm 45^\circ$ linear polarization basis. The rates for detection of $|3,0\rangle_{\pm 45^\circ}$ and $|2,1\rangle_{\pm 45^\circ}$ vary as $1 \pm \cos(3\phi)$, respectively. After passing through an 810 nm wavelength filter with a 10 nm passband, the photons enter the polarization analyzer, set to detect $|3,0\rangle_{\pm 45^\circ}$ or $|2,1\rangle_{\pm 45^\circ}$, as shown in Figure 1 b).

The use of down-converted pairs removes the need for detectors at the "dark" ports. Down-conversion very infrequently produces more than two photons in a single pulse so we can infer with near-certainty the absence of photons in the "dark" port from the presence of both photons in the "bright" port. Using a weak coherent state to supply the third photon, we can make small the probability that more than one LO photon was present in a triple detection event.[16] Thus a single post-selection for three-fold coincidence at the detectors performs at once the post-selections for both non-unitary operations.

Figure 2 shows results for detection of multiple polarizations at the analyzer. Intensities of the DC and LO sources were adjusted such that singles detections are mostly produced by LO photons (about 10:1 ratio vs. DC singles), two-fold coincidences mostly by DC pairs (about 5:1 vs. LO accidentals), and three-fold coincidences principally by one LO photon plus one DC pair (about 2:1 vs. accidental triples contributions, below). Thus

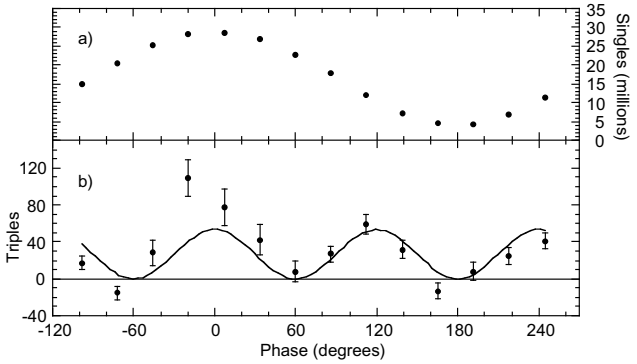

Figure 3. Super-resolving phase measurement with a single detected polarization. The polarization analyzer is configured to detect $|3,0\rangle_{\pm 45^\circ}$, i.e., with three detectors on the $+45^\circ$ channel. The input state is the same as in figure 2. Graphs show detections per 300 second counting interval as the phase ϕ is changed. a) singles detection shows oscillation with ϕ. b) three-fold coincidence detection (after background subtraction) shows oscillation with 3ϕ. Error bars show $\pm\sigma$ statistical uncertainty plus a systematic uncertainty in the background. Curve is the expected signal $A[1+\cos(3\phi)]$ with A chosen for best fit.

with a single scan of the phase shifter we can see qualitatively different behaviours for states of one, two, and three photons. Figure 2 c) clearly shows oscillation with 3ϕ, as predicted by theory. The resolution exceeds that achievable with any single photon in the experiment. The 405 nm photons would show oscillation with 2.1ϕ due to their shorter wavelength and the somewhat larger birefringence of quartz at that wavelength. The observed 3ϕ oscillation is analogous to multi-path interference: Because the DC and LO photons are indistinguishable, there are several different "paths" to the single outcome $|2,1\rangle_{\pm 45^\circ}$. For example, the LO photon could go to the -45° detector and the two DC photons to $+45^\circ$. This path interferes with other permutations to give the signal shown in Figure 2 c). A cosine curve fitted to these data shows a visibility of $42 \pm 3\%$. This visibility is unambiguous evidence of indistinguishability and entanglement among the three photons. A non-entangled state of three *distinguishable* photons could also show three-fold coincidence oscillation at 3ϕ, but with a maximal visibility of 20%.

Figure 2 d) shows the same triples data after subtraction of background from accidental triples. In addition to the signal of interest from 1 DC pair + 1 LO photon, we also see events from 2 DC pairs, from 3 LO photons, and from 2 LO photons + 1 DC pair. We calculate these backgrounds from independent measurements of single and double detection rates for the DC and LO sources alone. Coincidence background is calculated by the statistics of uncorrelated sources using a time-window of 12.5 ns, the laser pulse period. Incoherence of the various contributions is ensured by sweeping the path length of the LO photon over $\pm 2\mu m$ during acquisition. The calculated background has some variation with ϕ, so it is important to note that it is qualitatively different than the observed 3ϕ signal. Per 30 second interval, the accidental background contributes 22 ± 1 as a constant component, an average of 23 ± 1 oscillating with 2ϕ, 4 ± 1 with 1ϕ and < 1 with 3ϕ. Here and elsewhere, uncertainty in the counting circuitry's dead-time introduces a systematic error.

It is also possible to see 3ϕ behaviour detecting a single polarization, as shown in Figure 3. This measurement corresponds to the original proposals for atomic spectroscopy and lithography.[6,14] It gives a far weaker signal, in part because the maximum overlap of the state $|3::0\rangle^{3\phi}_{H,V}$ with $|3,0\rangle_{\pm 45^\circ}$ is smaller than with $|2,1\rangle_{\pm 45^\circ}$. Also, the chance that all three photons go to distinct detectors (as needed for coincidence detection) is smaller for $|3,0\rangle_{\pm 45^\circ}$. With these limitations, we are able to see the 3ϕ behaviour, but only by subtracting a considerable coincidence background.

Using linear optical elements and post-selection, we have constructed a multi-particle entangled state useful for super-resolving phase measurements. The demonstrated resolution is not only better than for a single infrared photon, it is better than could be achieved with any single photon in the experiment, including the down-conversion pump photons. Given the difficulty of generating coherent short-wavelength sources, this is encouraging for the prospects of proposals such as quantum-interferometric optical lithography. The method

can be adapted to generate entangled states of arbitrarily large photon number. Because prior entanglement is not required, the procedure would work well with single-photon-on-demand sources[31,32] which promise to be more efficient and scalable than down-conversion sources. Scalability would also be enhanced by the use of photon-number-resolving detectors. The construction proceeds from spatially separated, unentangled photons to a maximally-entangled state in a single spatial mode, a state suitable for Heisenberg-limited phase measurements.

3. NOON STATES IN PHASE ESTIMATION

The above demonstration of phase super-resolution is remarkable, and it is interesting to ask in what circumstances high resolution translates into high measurement precision, i.e., low uncertainty in the measured phase. The periodicity of the signal is of central importance here. For an N-photon NooN state, any observed signal has a period of $2\pi/N$, with the consequence that it provides information about the phase ϕ *modulo* $2\pi/N$. In order for the N-noon result to be unambiguous, it would appear that ϕ must already be localized to a $2\pi/N$ interval. In other words, in order to get $\sim 1/N$ precision one must already have $\sim 1/N$ precision. A similar situation holds for phase estimation with squeezed states, namely that squeezing can give higher precision, but only if the phase is already known to within about the phase uncertainty of the squeezed state. Similar observations have been made by Combes and Wiseman,[33] leading them to discount the utility of NooN states, at least for single-shot phase measurement.

We take as a point of reference the optimal phase measurements and optimal phase states described in the same paper.[33] For these states and measurements, the *single-shot* phase uncertainty is $\delta\phi = \pi/N$. These states, however, have not been produced in the laboratory, and it is unclear how the measurement, a probability-operator measure (POM) with an infinite number of possible outcomes, could be implemented. Our goal, then, is to understand how close to this optimal result one can arrive using NooN states, for which both production and measurement have been demonstrated in the experiment described above.

Our approach is to use a sequence of measurements with NooN states for phase estimation. In these "multi-shot" schemes, NooN states with a varying number of particles are used to obtain information with different periodicities. As we show, this can eliminate the ambiguities while retaining the high-resolution information. The result is phase estimation with the "Heisenberg-limited" scaling of $\delta\phi \propto 1/N$.

We change notation slightly, such that the NooN state is now written

$$|N,\theta\rangle_{a,b} \equiv \frac{1}{\sqrt{2}}(|N,0\rangle_{a,b} + e^{i\theta}\,|0,N\rangle_{a,b}) \tag{4}$$

where $|n_a, n_b\rangle$ indicates a Fock state with $n_a.n_b$ photons in two orthogonal modes a and b, respectively. A phase shift of ϕ applied to each particle in the b state rotates the second component by $N\phi$ relative to the first, so that the shifted state is

$$|N,\theta\rangle_{a,b} \xrightarrow{\phi} |N,\theta+N\phi\rangle_{a,b} \tag{5}$$

The N-fold amplification of the phase is responsible for super-resolution: any observable on this state will be periodic in ϕ with a period of at most $2\pi/N$. Experimentally, a convenient measurement is projection onto Fock states in a rotated basis. This can be accomplished by bringing the two modes together on a beamsplitter followed by single photon detectors. Defining the modes $c \equiv (a+b)/\sqrt{2}$ and $d \equiv (a-b)/\sqrt{2}$, we find that the probabilities $P_N(n_d|\theta)$ are

$$\begin{aligned} P_N(n_d|\theta) &= |\,\langle N-n_d, n_d|N,\theta\rangle_{a,b}\,|^2 \\ &= \frac{1\pm\cos(\theta)}{2^N}\begin{pmatrix} N \\ n_c \end{pmatrix} \end{aligned} \tag{6}$$

where the plus (minus) sign applies if n_d is even (odd). For the purposes of estimating the phase, there are effectively only two outcomes, n_d even ("0") or n_d odd ("1"), with probabilities $P_N(0|\theta) = [1+\cos(\theta)]/2$ and $P_N(1|\theta) = [1-\cos(\theta)]/2$, respectively.

Phase estimation proceeds by making successive refinements to a probability distribution function $f(\phi)$ for the unknown phase ϕ. Before any measurements are made, it is assumed that $f_0(\phi) = 1/2\pi$ is a constant,

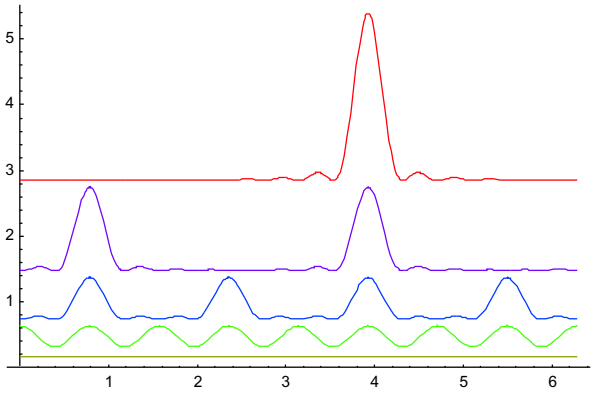

Figure 4. Illustration of phase estimation by the "binary elimination" scheme. Curves show the probability density function after zero (bottom curve) to four (top curve) measurements. Curves have been offset for clarity. The first measurement uses $N = 8$, leaving eight peaks, the second uses $N = 4$, and so forth. Note that the strategy is adaptive: the phase of each measurement depends on information from previous measurements.

indicating complete ignorance about the phase to be estimated. Each measurement consists of the input of a NooN state with photon number N_i and initial phase θ_i, rotation by the unknown phase ϕ and measurement in the $\{c, d\}$ basis with the measured result r_i being 0 or 1. The marginal probability distribution is updated as

$$f_i(\phi) = P_N(r_i|N_i\phi + \theta_i)f_{i-1}(\phi)/Z. \tag{7}$$

Where Z is a normalization constant. In the language of Baysian estimation, $P_N(r_i|N_i\phi + \theta_i)$ is the likelihood function for the phase ϕ given the outcome r_i.

To measure the success of an estimation procedure we use the "sharpness"

$$Sh \equiv |\left\langle e^{i\phi}\right\rangle_f| = |\int d\phi f(\phi)e^{i\phi}| \tag{8}$$

which is related to the phase variance by $\delta\phi^2 = 2(1 - Sh) = (1 - Sh^2)$ in the limit of narrow distributions.

Given a total of $N_{\rm tot}$ photons to use for the phase estimation, can a measurement sequence $\{(N_i, \theta_i)\}$ give a narrow marginal distribution $f(\phi)$? Use of all the photons in a single $|N_{\rm tot}, \theta\rangle$ state does not work for this purpose. The resulting distribution oscillates rapidly but remains spread over the whole of the phase range.

Before describing our solution, we first describe a strategy, binary elimination, which comes close to solving the problem and which serves to illustrate the main points. If $N_{\rm tot} = 2^n - 1$ photons are available, the first 2^{n-1} are used in the first measurement, leaving a marginal distribution with 2^{n-1} peaks. The next measurement, with 2^{n-2} photons, leaves 2^{n-2} peaks, and so on, until a single peak is left. This procedure is necessarily adaptive, the input phase for each measurement must be chosen to align with the peaks left by the measurement before. Explicitly, $N_i = 2^{n-i}$, $\theta_1 = 0$ and $\theta_i = (\theta_{i-1} + \pi r_{i-1})/2$. Binary elimination is guaranteed to give a single peak, one out of 2^n possibilities, but the peak is not especially narrow: the phase variance limits to $\delta\phi^2 \equiv \int d\phi\,(\phi - \langle\phi\rangle)^2 = 1/N_{\rm tot}$, the same as the shot noise limit.

We now describe a truly successful strategy which uses only NooN states and number state detection and which gives phase estimates better than the shot noise limit. Indeed, the strategy appears to reach the "Heisenberg limit" scaling of $\delta\phi^2 \to A/N_{\rm tot}^2$, with A not much larger than for the ideal strategy. As with the binary elimination, this strategy is adaptive. First, as an initialization step, a small number of $N = 1$ NooN measurements (i.e., measurements with single particles) are made. In our case we used 100 such single-particle measurements to get a roughly gaussian distribution of width $\delta\phi \approx 1/10$. In subsequent steps, the prior distribution $f_{i-1}(\phi)$ is used to choose the most appropriate value of N_i for the next (ith) measurement. Speicificallly, N_i is chosen to minimize $\langle S\rangle / \ln N_{\rm tot}^{(i)}$ where $N_{\rm tot}^{(i)} = \sum_{j=1}^{i} N_j$ and $\langle S\rangle$ is the entropy $S \equiv -\int d\phi f_i(\phi) \ln f_i(\phi)$ averaged over the

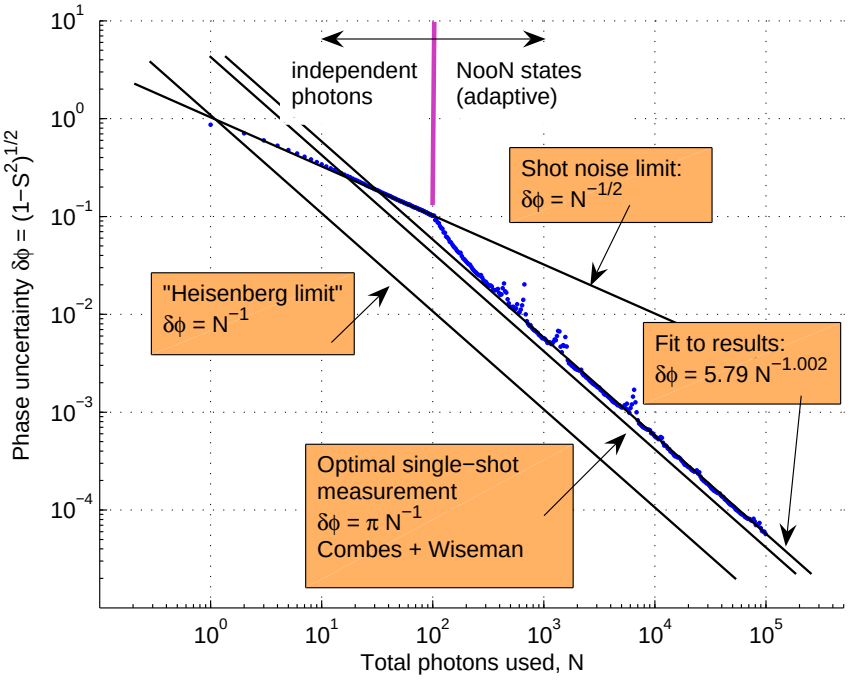

Figure 5. Results of Monte-Carlo simulation of adaptive, multi-shot phase estimation with NooN states. In each run, the first 100 particles were used for single-particle measurements, giving the shot-noise limit as evidenced by the slope of -1/2. The continuation of each run implemented an adpative strategy (see text), and shows a steeper slope, consistent with -1. Each dot shown indicates an average over 1000 runs.

two possible outcomes. In all measurements, including the single-particle initialization steps, the input phase θ_i is chosen such that the two outcomes are equally likely.

Monte-Carlo simulation of this problem is simple and efficient. The Fourier representation

$$f(\phi) = \sum_{m=-\infty}^{\infty} g_m e^{im\phi} \tag{9}$$

is convenient for numerical simulations because the various averages can be simply expressed in terms of the coefficients g_m. For example, $\langle e^{i\phi} \rangle_f = g_1/g_0$ and $\mu_4 \approx 2(3g_0 - 4|g_1| + |g_1|^2 \mathrm{Re}[g_2/g_1^2])/g_0$.

In practice, the marginal distribution tends to nearly Gaussian, and we used the Gram-Charlier expansion to approximate the entropy in terms of the of moments $\mu_k \equiv \int d\phi\, (\phi - \langle\phi\rangle)^k f(\phi)$ as

$$S \approx -\frac{1}{2}(1 + \ln 2\pi + \ln \mu_2) + \frac{1}{12}\mu_3^2 + \frac{1}{48}(\mu_4 - 3\mu_2^2)^2. \tag{10}$$

Note that while S is approximated, the probability distribution function $f(\phi)$ is exact. The strategy above was simulated for 1000 realizations, stopping each realization when N_{tot} exceeded 10^5.

Results are shown in Figure 5. For comparison, the best single-measurement phase variance[33] of $\delta\phi^2 = \pi^2/N^2$ is shown as a solid line.

Fitting to the lower part of the curve, for $N_{tot}^{(i)} \geq$??? we obtain the scaling

$$\sqrt{2(1 - Sh)} = AN^{-\beta} \tag{11}$$

with A =???±??? and β =???±???. For comparison, the best single-measurement phase uncertainty is only slightly more precise: $\sqrt{2(1-Sh)} = \pi/N$.

Simulations for various starting conditions work equally well.

In conclusion, we have presented an adaptive, multi-shot phase estimation technique which uses only "NooN" entangled states, phase shifters, beamsplitters, and single-photon detectors, and which achieves a phase uncertainty better than the shot noise limit for general starting conditions. The strategy achives phase uncertainty which scales as one over the total number of photons used, and is less than a factor of two less precise than the optimal single-shot phase estimation strategy, which requires preparation of more complicated states and generalized phase measurements which have not been demonstrated experimentally.

4. ACKNOWLEDGEMENTS

We thank K. Resch, J. O'Brien, R. Muñoz-Tapies and E. Bagan for helpful discussions. This work was supported by the National Science and Engineering Research Council of Canada, Photonics Research Ontario, the Canadian Institute for Photonic Innovations, the DARPA-QuIST program, and ICFO.

This document shows the desired format and appearance of a manuscript prepared for the Proceedings of the SPIE.* It is prepared using LaTeX2e[34] with the class file `spie.cls`. The LaTeX source file used to create this document is `article.tex`, which contains important formatting information embedded in it. These files are available on the Internet at `http://home.lanl.gov/kmh/spie/`. The font used throughout is the LaTeX default font, Computer Modern Roman, which is equivalent to the Times Roman font available on many systems. If this font is not available, use a similar serif font. Normal text has a font size of 10 points† for which the actual height of a capital E is about 2.4 mm (7 pt.) and the line-to-line spacing is about 4.2 mm (12 pt.). The font attributes for other parts of the manuscript, summarized in Table 1, are described in the following sections. Normal text should be justified to both the left and right margins. Appendix B has information about PostScript fonts.

To be properly reproduced in the Proceedings, all text and figures must fit inside a rectangle 6.75-in. wide by 8.75-in. high or 17.15 cm by 22.23 cm. The text width and height are set in `spie.cls` to match this requirement. The text should begin 1.00 in. or 2.54 cm from the top of the page. The right and left margins should be

Table 1. Fonts sizes to be used for various types of text. All fonts are Computer Modern Roman or an equivalent. Table captions should be centered above the table. When the caption is too long to fit on one line, it should be justified to the right and left margins of the body of the text.

Article title	16 pt., bold, centered
Author names and affiliations	12 pt., normal, centered
Section heading	11 pt., bold, centered (all caps)
Subsection heading	11 pt., bold, left justified
Sub-subsection heading	10 pt., bold, left justified
Normal text	10 pt., normal
Figure and table captions	9 pt., normal
Footnote	9 pt., normal

0.875 in. or 2.22 cm for US letter-size paper (8.5 in. by 11 in.) or 1.925 cm for A4 paper (210 mm by 297 mm) to horizontally center the text on the page. See Appendix B for guidance regarding paper-size specification.

Authors are encouraged to follow the principles of sound technical writing, as described in Ref. 35, for example. Many aspects of technical writing are addressed in the *AIP Style Manual*, published by the American Institute of Physics. It is available on line at `http://www.aip.org/pubservs/style/4thed/toc.html`. Good English usage is essential. A spelling checker is helpful for finding misspelled words.

An author may use this LaTeX source file as a template by substituting his/her own text in each field. This document is not meant to be a complete guide on how to use LaTeX. For that, refer to books on LaTeX usage, such as the definitive work by Lamport[34] or the very useful compendium by Goossens et al.[36]

5. PARTS OF MANUSCRIPT

This section describes the normal structure of a manuscript and how each part should be handled. The appropriate vertical spacing between various parts of this document is achieved in LaTeX through the proper use of defined constructs, such as `\section{}`. In LaTeX, paragraphs are separated by blank lines in the source file.

At times it may be desired, for formatting reasons, to break a line without starting a new paragraph. This situation may occur, for example, when formatting the article title, author information, or section headings. Line breaks are inserted in LaTeX by entering \\ or `\linebreak` in the LaTeX source file at the desired location.

*This format was developed in 1995 by Rick Herman, SPIE, and Ken Hanson, Los Alamos National Laboratory.

†Font sizes are specified in points, abbreviated pt., which is a unit of length. One inch = 72.27 pt.; one cm = 28.4 pt.

5.1. Title and Author Information

The article title appears centered at the top of the first page. The title font is 16 point, bold. The rules for capitalizing the title are the same as for sentences; only the first word, proper nouns, and acronyms should be capitalized. Avoid using acronyms in the title, unless they are widely understood. Consider the possibility that people outside your area of expertise might read your article. Appendix A contains more about acronyms.

The list of authors immediately follows the title after a blank vertical space of about 7 mm. The font is 12 point, normal with each line centered. The authors' affiliations and addresses follow the author list after another blank space of about 4 mm, also in 12-point, normal font and centered. Do not use acronyms in affiliations and addresses. For multiple affiliations, each affiliation should appear on a new line, separated from the following address by a semicolon. Italicized superscripts may be used to identify the correspondence between the authors and their respective affiliations. Further author information, such as e-mail address, complete postal address, and web-site location, may be provided in a footnote by using `\authorinfo{}`, as demonstrated above.

When the abbreviated title or author information is too long to fit on one line, multiple lines may be used; insert line breaks appropriately to achieve a visually pleasing format. The proper spacing of one and one-half lines between the title, author list, and their affiliations is achieved with the LaTeX command `\skiplinehalf` defined in `spie.cls`.

5.2. Abstract and Keywords

The title and author information is immediately followed by the Abstract. The Abstract should concisely summarize the key findings of the paper. It should consist of a single paragraph containing no more than 200 words. The Abstract does not have a section number. A list of up to ten keywords should immediately follow the Abstract after a blank line. These keywords will be included in a searchable database at SPIE.

5.3. Body of Paper

The body of the paper consists of numbered sections that present the main findings. These sections should be organized to best present the material. See Sect. 6 for formatting instructions.

5.4. Appendices

Auxiliary material that is best left out of the main body of the paper, for example, derivations of equations, proofs of theorems, and details of algorithms, may be included in appendices. Appendices are enumerated with upper-case Latin letters in alphabetic order, and appear just before the Acknowledgments and References.

5.5. Acknowledgments

In the Acknowledgments section, appearing just before the References, the authors may credit others for their guidance or help. Also, funding sources may be stated. The Acknowledgments section does not have a section number.

5.6. References

The References section lists books, articles, and reports that are cited in the paper. It does not have a section number. The references are numbered in the order in which they are cited. Examples of the format to be followed are given at the end of this document.

The reference list at the end of this document is created using BibTeX, which looks through the file `report.bib` for the entries cited in the LaTeX source file. The format of the reference list is determined by the bibliography style file `spiebib.bst`, as specified in the `\bibliographystyle{spiebib}` command. Alternatively, the references may be directly formatted in the LaTeX source file.

For books[34–37] the listing includes the list of authors, book title (in italics), page or chapter numbers, publisher, city, and year of publication. A reference to a journal article[38] includes the author list, title of the article (in quotes), journal name (in italics, properly abbreviated), volume number (in bold), inclusive page numbers, and year. By convention,[34] article titles are capitalized as described in Sect. 5.1. A reference to

a proceedings paper or a chapter in an edited book[39] includes the author list, title of the article (in quotes), conference name (in italics), if appropriate, editors, volume or series title (in italics), volume number (in bold), if applicable, inclusive page numbers, publisher, city, and year. References to an article in the SPIE Proceedings may include the conference name, as shown in Ref. 40.

Citations to the references are made using superscript numerals, as demonstrated in the preceding paragraph. One may also directly refer to a reference within the text, e.g., "as shown in Ref. 38 ..." Footnotes[‡] may be used to provide auxiliary information that doesn't need to appear in the text, e.g., to explain measurement units. They should be used sparingly, however. Since only nine symbols are available, you may need to restart the sequence with the first sybmol using the command `\footnote[1]{Your footnote text goes here.}`.

6. SECTION FORMATTING

Section headings are centered and formatted completely in upper-case 11-point bold font. Sections should be numbered sequentially, starting with the first section after the Abstract. The heading starts with the section number, followed by a period. In LaTeX, a new section is created with the `\section{}` command, which automatically numbers the sections.

Paragraphs that immediately follow a section heading are leading paragraphs and should not be indented, according to standard publishing style.[34] The same goes for leading paragraphs of subsections and sub-subsections. Subsequent paragraphs are standard paragraphs, with 14-pt. (5 mm) indentation. An extra half-line space should be inserted between paragraphs. In LaTeX, this spacing is specified by the parameter `\parskip`, which is set in `spie.cls`. Indentation of the first line of a paragraph may be avoided by starting it with `\noindent`.

6.1. Subsection Attributes

The subsection heading is left justified and set in 11-point, bold font. Capitalization rules are the same as those for book titles. The first word of a subsection heading is capitalized. The remaining words are also capitalized, except for minor words with fewer than four letters, such as articles (a, an, and the), short prepositions (of, at, by, for, in, etc.), and short conjunctions (and, or, as, but, etc.). Subsection numbers consist of the section number, followed by a period, and the subsection number within that section, followed by a period.

6.1.1. Sub-subsection attributes

The sub-subsection heading is left justified and its font is 10 point, bold. Capitalize as for sentences. The first word of a sub-subsection heading is capitalized. The rest of the heading is not capitalized, except for acronyms and proper names.

7. FIGURES AND TABLES

Figures are numbered in the order of their first citation. They should appear in numerical order and on or after the same page as their first reference in the text. Alternatively, all figures may be placed at the end of the manuscript, that is, after the Reference section. It is preferable to have figures appear at the top or bottom of the page. Figures, along with their captions, should be separated from the main text by at least 0.2 in. or 5 mm.

Figure captions are centered below the figure or graph. Figure captions start with the figure number in 9-point bold font, followed by a period; the text is in 9-point normal font; for example, "**Figure 3.** Original image...". See Fig. 6 for an example of a figure caption. When the caption is too long to fit on one line, it should be justified to the right and left margins of the body of the text.

Tables are handled identically to figures, except that their captions appear above the table.

For further details concerning the inclusion of grayscale and color images, consult the *Author Guide for Publication and Presentation* supplied to authors by SPIE or SPIE's web page on manuscript preparation.

[‡]Footnotes are indicated as superscript symbols to avoid confusion with citations.

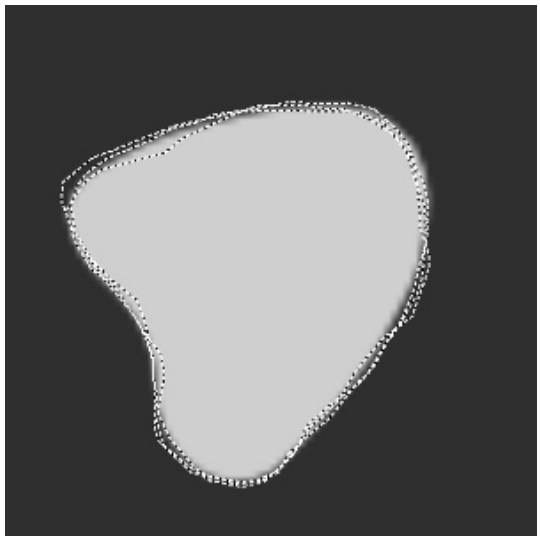

Figure 6. Figure captions are used to label the figure and help the reader understand the figure's significance. The caption should be centered underneath the figure and set in 9-point font. It is preferable for figures and tables to be placed at the top or bottom of the page. LaTeX tends to adhere to this standard.

APPENDIX A. MISCELLANEOUS FORMATTING DETAILS

It is often useful to refer back (or forward) to other sections in the article. Such references are made by section number. When a section reference starts a sentence, Section is spelled out; otherwise use its abbreviation, for example, "In Sect. 2 we showed..." or "Section 2.1 contained a description...". References to figures, tables, and theorems are handled the same way.

At the first occurrence of an acronym (unless it is widely known, such as MTF, CCD, FFT), spell it out, followed by the acronym in parentheses, e.g., noise power spectrum (NPS).

A.1. Formatting Equations

Equations may appear in line with the text, if they are simple, short, and not of major importance; e.g., $\beta = b/r$. Important equations appear on their own line. Such equations are centered. For example, "The expression for the minus-log-posterior is

$$\phi = |\mathbf{y} - \mathbf{A}\mathbf{x}|^2 + \alpha \log p(\mathbf{x}) \,, \tag{12}$$

where α determines the strength of ..." Principal equations are numbered, with the equation number placed within parentheses and right justified.

Equations are considered to be part of a sentence and should be punctuated accordingly. In the above example, a comma follows the equation because the next line is a subordinate clause. If the equation ends the sentence, a period should follow the equation. The line following an equation should not be indented unless it is meant to start a new paragraph. Indentation after an equation is avoided in LaTeX by not leaving a blank line between the equation and the subsequent text.

References to equations include the equation number in parentheses, for example, "Equation (12) shows ..." or "Combining Eqs. (2) and (3), we obtain..." Using a tilde in the LaTeX source file avoids unwanted line breaks.

A.2. Formatting Theorems

To include theorems in a formal way, the theorem identification should appear in a 10-point, bold font, left justified and followed by a period. The text of the theorem continues on the same line in normal, 10-point font. For example,

Theorem 1. For any unbiased estimator...

Formal statements of lemmas and algorithms receive a similar treatment.

APPENDIX B. SOME LATEX GUIDANCE

SPIE has had a number of problems with manuscripts submitted electronically as PostScript (PS) files that were prepared by LaTeX. The major problem has been incorrect margins at the top of each page, which seems to be related to the document's paper size. The paper size is set at two separate places in the process of creating a PS file. The first step in this process is to run `latex` on the LaTeX source file, together with the class file `spie.cls`. The default in `article.cls`, on which `spie.cls` is based, is USA letter paper. To format a document for A4 paper, the first line of the LaTeX source file should be `\documentclass[a4paper]{spie}`.

The output of the LaTeX utility is a file with the extension DVI (for Device Independent), which encodes the formatted document. The application DVIPS is typically used to convert the DVI file to a PS file. DVIPS has its own default paper size, which can be overridden with the option "`-t letter`" or "`-t a4`". If the foregoing steps do not produce the correct top margin, you can lower the text on the page (by 9 mm) with the command `\addtolength{\voffset}{9mm}`, placed right after the `\documentclass` command.

Another DVIPS option specifies the incorporation of (scalable) PostScript Type 1 fonts in its output PS file. This feature is important for obtaining a subsequent PDF file that will be clearly displayed on a computer monitor by Adobe Acrobat Reader. The option "`-P pdf`" makes DVIPS include these fonts in its output PS file.

ACKNOWLEDGMENTS

This unnumbered section is used to identify those who have aided the authors in understanding or accomplishing the work presented and to acknowledge sources of funding.

REFERENCES

1. N. F. Ramsey, "The method of successive oscillatory fields," *Phys. Today* **33**(7), pp. 25–30, 1980.
2. W. H. Bragg and W. L. Bragg, "The reflection of x-rays by crystals," *Proc. Roy. Soc. London* **88**, pp. 428–438, 1913.
3. B. C. Barish and R. Weiss, "LIGO and the detection of gravitational waves," *Phys. Today* **52**, pp. 44–50, Oct 1999.
4. B. Caron, A. Dominjon, C. Drezen, R. Flaminio, X. Grave, V. Ferrari, E. Majorana, P. Puppo, P. Rapagnani, and F. Ricci, "The Virgo interferometer," *Class. Quantum Gravity* **14**, pp. 1461–1469, Jun 1997.
5. M. J. Holland and K. Burnett, "Interferometric detection of optical-phase shifts at the Heisenberg limit," *Phys. Rev. Lett.* **71**, pp. 1355–1358, Aug 30 1993.
6. J. J. Bollinger, W. M. Itano, D. J. Wineland, and D. J. Heinzen, "Optimal frequency measurements with maximally correlated states," *Phys. Rev. A* **54**, pp. R4649–R4652, Dec 1996.
7. Z. Y. Ou, "Fundamental quantum limit in precision phase measurement," *Phys. Rev. A* **55**, pp. 2598–2609, Apr 1997.
8. J. P. Dowling, "Correlated input-port, matter-wave interferometer: Quantum-noise limits to the atom-laser gyroscope," *Phys. Rev. A* **57**, pp. 4736–4746, Jun 1998.
9. R. A. Campos, C. C. Gerry, and A. Benmoussa, "Optical interferometry at the Heisenberg limit with twin Fock states and parity measurements," *Phys. Rev. A* **68**, p. 023810, Aug 2003.
10. M. D'Angelo, M. V. Chekhova, and Y. Shih, "Two-photon diffraction and quantum lithography," *Phys. Rev. Lett.* **8701**, p. 013602, Jul 2 2001.
11. C. A. Sackett, D. Kielpinski, B. E. King, C. Langer, V. Meyer, C. J. Myatt, M. Rowe, Q. A. Turchette, W. M. Itano, D. J. Wineland, and I. C. Monroe, "Experimental entanglement of four particles," *Nature* **404**, pp. 256–259, Mar 16 2000.
12. A. Rauschenbeutel, G. Nogues, S. Osnaghi, P. Bertet, M. Brune, J. M. Raimond, and S. Haroche, "Step-by-step engineered multiparticle entanglement," *Science* **288**, pp. 2024–2028, Jun 16 2000.

13. Z. Zhao, T. Yang, Y. A. Chen, A. N. Zhang, M. Zukowski, and J. W. Pan, "Experimental violation of local realism by four-photon Greenberger-Horne-Zeilinger entanglement," *Phys. Rev. Lett.* **91**, p. 180401, Oct 31 2003.
14. P. Kok, H. Lee, and J. P. Dowling, "Creation of large-photon-number path entanglement conditioned on photodetection," *Phys. Rev. A* **65**, p. 052104, May 2002.
15. J. Fiurasek, "Conditional generation of n-photon entangled states of light," *Phys. Rev. A* **65**, p. 053818, May 2002.
16. G. J. Pryde and A. G. White, "Creation of maximally entangled photon-number states using optical fiber multiports," *Phys. Rev. A* **68**(5), p. 052315, 2003.
17. H. F. Hofmann, "Generation of highly nonclassical n-photon polarization states by superbunching at a photon bottleneck," *Phys. Rev. A* **70**(2), p. 023812, 2004.
18. E. Knill, R. Laflamme, and G. J. Milburn, "A scheme for efficient quantum computation with linear optics," *Nature* **409**, pp. 46–52, Jan 4 2001.
19. J. D. Franson, M. M. Donegan, M. J. Fitch, B. C. Jacobs, and T. B. Pittman, "High-fidelity quantum logic operations using linear optical elements," *Phys. Rev. Lett.* **89**, p. 137901, Sep 23 2002.
20. K. J. Resch, J. S. Lundeen, and A. M. Steinberg, "Conditional-phase switch at the single-photon level," *Phys. Rev. Lett.* **89**, p. 037904, Jul 15 2002.
21. M. W. Mitchell, C. W. Ellenor, S. Schneider, and A. M. Steinberg, "Diagnosis, prescription, and prognosis of a Bell-state filter by quantum process tomography," *Phys. Rev. Lett.* **91**, p. 120402, Sep 19 2003.
22. J. L. O'Brien, G. J. Pryde, A. G. White, T. C. Ralph, and D. Branning, "Demonstration of an all-optical quantum controlled-NOT gate," *Nature* **426**, pp. 264–267, Nov 20 2003.
23. B. C. Sanders, G. J. Milburn, and Z. Zhang, "Optimal quantum measurements for phase-shift estimation in optical interferometry," *J. Mod. Opt.* **44**, pp. 1309–1320, Jul 1997.
24. S. F. Huelga, C. Macchiavello, T. Pellizzari, A. K. Ekert, M. B. Plenio, and J. I. Cirac, "Improvement of frequency standards with quantum entanglement," *Phys. Rev. Lett.* **79**, pp. 3865–3868, Nov 17 1997.
25. J. G. Rarity, P. R. Tapster, E. Jakeman, T. Larchuk, R. A. Campos, M. C. Teich, and B. E. A. Saleh, "2-photon interference in a Mach-Zehnder interferometer," *Phys. Rev. Lett.* **65**, pp. 1348–1351, Sep 10 1990.
26. Z. Y. Ou, X. Y. Zou, L. J. Wang, and L. Mandel, "Experiment on nonclassical 4th-order interference," *Phys. Rev. A* **42**, pp. 2957–2965, Sep 1 1990.
27. V. Meyer, M. A. Rowe, D. Kielpinski, C. A. Sackett, W. M. Itano, C. Monroe, and D. J. Wineland, "Experimental demonstration of entanglement-enhanced rotation angle estimation using trapped ions," *Phys. Rev. Lett.* **86**, pp. 5870–5873, Jun 25 2001.
28. J. G. Rarity, P. R. Tapster, and R. Loudon, "Nonclassical interference between independent sources," Preprint at (http::/arxiv.org/quant-ph/9702032) , 1997.
29. J. G. Rarity and P. R. Tapster, "Three-particle entanglement from entangled photon pairs and a weak coherent state," *Phys. Rev. A* **59**, pp. R35–R38, Jan 1999.
30. S. Takeuchi, "Beamlike twin-photon generation by use of type II parametric downconversion," *Opt. Lett.* **26**, pp. 843–845, Jun 1 2001.
31. P. Michler, A. Kiraz, C. Becher, W. V. Schoenfeld, P. M. Petroff, L. D. Zhang, E. Hu, and A. Imamoglu, "A quantum dot single-photon turnstile device," *Science* **290**, pp. 2282–2285, Dec 22 2000.
32. G. S. Solomon, M. Pelton, and Y. Yamamoto, "Single-mode spontaneous emission from a single quantum dot in a three-dimensional microcavity," *Phys. Rev. Lett.* **86**, pp. 3903–3906, Apr 23 2001.
33. J. Combes and H. M. Wiseman, "States for phase estimation in quantum interferometry," *JOURNAL OF OPTICS B-QUANTUM AND SEMICLASSICAL OPTICS* **7**(1), pp. 14–21, 2005.
34. L. Lamport, *LaTeX: A Document Preparation System*, Addison-Wesley, Reading, Mass., 1994.
35. A. Eisenberg, *Guide to Technical Editing*, Oxford University, New York, 1992.
36. M. Goossens, F. Mittelbach, and A. Samarin, *The LaTeX Companion*, Addison-Wesley, Reading, Mass., 1997.
37. A. Gelman, J. B. Carlin, H. S. Stern, and D. B. Rubin, *Bayesian Data Analysis*, Chapman & Hall, London, 1995.

38. N. Metropolis, A. W. Rosenbluth, M. N. Rosenbluth, A. H. Teller, and E. Teller, "Equations of state calculations by fast computing machine," *J. Chem. Phys.* **21**, pp. 1087–1091, 1953.
39. S. F. Gull, "Developments in maximum-entropy data analysis," in *Maximum Entropy and Bayesian Methods*, J. Skilling, ed., pp. 53–71, Kluwer Academic, Dordrecht, 1989.
40. K. M. Hanson, "Introduction to Bayesian image analysis," in *Medical Imaging: Image Processing*, M. H. Loew, ed., *Proc. SPIE* **1898**, pp. 716–731, 1993.